Study of $Y_1Ba_2Cu_3O_{7-\delta}$+CuO nanocomposite as a resistive current limiter

A.V. Ushakov[a,b], I.V. Karpov[a,b], V.G. Demin[a,b], A.A. Shaihadinov[a,b], A.I. Demchenko[b], E.P. Bachurina[a,b]

[a] Krasnoyarsk Scientific Center of the Siberian Branch of the Russian Academy of Science, Krasnoyarsk 660036, Russia

[b] Siberian Federal University, Krasnoyarsk, 660041, Russia

* Corresponding author. E-mail address: sfu-unesco@mail.ru

Abstract. The influence of CuO nanoscale inclusions as the second component of the composites on the transport properties of superconducting polycrystals $YBa_2Cu_3O_7$ was studied. Samples of $YBa_2Cu_3O_{7-\delta}$ with different content of CuO nanoparticles were synthesized. The analysis of magnetic properties was carried out within the framework of the extended critical state model. It was found that the addition of 20 wt.% CuO nanoparticles leads to an increase in the critical current density at T = 77 K. A further increase to 30 wt.% reduces the critical current density. The results of the experimental studies of a switching superconducting fault current limiter in AC voltage networks based on high-temperature superconductors (HTSC) of the 2nd generation are given in this work. The testing equipment contains a series-connected HTSC module and a high-speed current switch with a break time of 9 ms. The high efficiency of the samples made from the $YBa_2Cu_3O_{7-\delta}$ + CuO nanocomposite material as an active element of a resistive current limiter is shown.

Keywords: YBCO ceramics, critical current, current limiter.

Introduction. One of the promising ways of limiting fault currents (FC) could be the creation of current-limiting devices based on high-temperature superconductors (HTSC) of the 2nd generation. Such materials, in comparison with previous-generation superconductors, are characterized by reduced metal content (small thickness of the substrate and stabilizer), additional heat removal, a higher critical current value and a high resistance to emergency currents in a normal state. In normal operation, the device has practically no influence on the mode of the system, while in emergency operation, it introduces the resistance, necessary to limit the fault current to the required level, into the network.

Based on design features, two basic concepts of a superconducting current limiter (SCL) can be distinguished: resistive and inductive. Other schematic solutions are based on these concepts [1, 2]. In the case of inductive design, the magnetic coupling between the superconducting element and the winding is carried out through a three-core magnetic conductor [3]. For example, the ABB company developed three-phase current limiter (1.2 MVA) with a cylindrical screen consisting of 16 rings which were made from the superconducting ceramics Bi-2212, which was tested and operated during the year [4]. The operation of an inductive current limiter is concerned with the presence of magnetic stray fields, which can adversely affect the use of a metal cryostat and increase power loss.

The resistive design of a superconducting current limiter is based on the nonlinearity of the superconductor resistance and it could use massive elements or coils [5]. When superconducting coils are used as superconducting elements, they are arranged in such a way to make the total inductance of the limiter possibly minimal [6]. A resistive superconducting current limiter contains a HTSC module placed in a cryostat with liquid or supercooled nitrogen, acting as a cooling agent,

and high-voltage current inputs of a special design. The basic disadvantage of a resistive superconducting current limiter is considerable heat generation, the presence of magnetic stray fields, overheating during a short circuit, and a relatively long response time.

The paper [7] describes the development of composite material based on the $YBa_2Cu_3O_{7-\delta}$ granular superconductor and CuO electric arc nanopowders [8–12]. The addition of CuO nanopowders improves the quality of the sintered composites, with significant increase in the critical current density, as well as a peak effect in the region of strong magnetic fields [13]. Changing the concentration of CuO nanopowders make it possible to achieve a smooth regulation of the critical current density and a decrease in the transition time to the normal state.

This paper presents the results of measurements of the parameters of a polycrystalline (ceramic) HTSC device connected in accordance with the series subcircuit in the current limiting mode to 1000 A during the first half-wave of an alternating current. Theoretically, such a ballast resistance at a transport current less than the critical (J_c) is equal to zero and, when an emergency situation occurs, accompanied by an increase in current above J_c, it "switches on" into the circuit and limits the current to a given value. In the practical implementation of such a limiter, it is necessary to overcome a number of technical challenges, among them are the problem of contacts in HTSC, the problem of heat removal from the HTSC protection element in the short circuit protection mode (when the HTSC remains the only consumer) and the resulting task of negotiating the HTSC element according to the voltage drop in the resistive state with the voltage of the protected circuit, which determines its geometrical dimensions and the power developed in a unit of volume.

The samples for measurements were made by pressing and sintering the prepared HTSC powder $YBa_2Cu_3O_{7-\delta}$ with CuO nanoparticles coated on the surface. The synthesis of $YBa_2Cu_3O_{7-\delta}$ + CuO composites is described in [14]. During the experiment, the samples with 10, 20 and 30 wt.% CuO were used. The samples were protected on the top with a layer of silver with a thickness of about 2 microns without a stabilizing copper shell, which is better suited for use in resistive superconducting current limiters, since they have the highest resistance in a normal non-superconducting state. The typical sample size was 2×7×44 mm. To increase the area to the maximum possible, the current contacts were covered with In – Ga eutectic. The assembled unit was placed in a bath with liquid nitrogen. The studies were conducted on a low-voltage testing equipment, which contained a transformer with an output voltage U_0 = 20 V (rms value), a network key K_1 with an electromagnetic drive, a load resistance R_0 = 0.2 Ω, and a control system (Fig. 1). A chain with the connected in series thyristor key *VT* and the additional resistance R_1 was wired parallel to the R_0 resistance. The key *VT* was used to simulate the occurrence of fault current, the amplitude of which was regulated by changing the resistance R_1. The test samples R_{HTSC} and switch K_2 were connected to the output of the transformer before the load resistance R_0. During the experiments, the HTSC samples were immersed in a Dewar vessel filled with liquid nitrogen.

The control system (CS) generated signals with an adjustable turn-on delay K_1 at the moment of circuit voltage maximum, turn-on *VT* to generate a fault current approximately one period after the start of the load current flow, and turn-off K_2 at the end of the first half-wave of the current. The expected amplitude of the first half-wave of the fault current was 4700 A.

To study the recovery mode of the superconducting element of the HTSC after the current was turned off by the K_2 switch, it was shunted by resistance R_2. The total duration of current flow in the HTSC element was about 300 ms.

The inherent resistance of the low-voltage network in the fault mode was lower (less than 15 mOhm) compared with the resistance of HTSC elements after the transition to the normal state.

Therefore, almost all the circuit voltage was applied to HTSC. Such conditions are close to the actual conditions of current limitation in AC networks with a given voltage. The change in the parameters of the current limitation was regulated by changing the additives of CuO nanodispersed powder.

For each sample, oscillographic testing of current and voltage was performed. The limited current i_{lim} was measured by a galvanically isolated sensor with a sensitivity of 2560 A/V The electrical signals were recorded using P6139A testers on a Tektronix DPO 4034 oscillograph, and then they were saved and processed on a personal computer. While being processed on a computer, the inductive component of the voltage drop on the HTSC element was subtracted from the measurement data.

The magnetic measurements were carried out with the MPMS-XL5 unit. Debye X-ray patterns were recorded on the D8 ADVANCE diffractometer (Bruker AXS). The measurements of the isothermal dependences of the magnetization on the magnetic field were carried out at a temperature of 77 K. The critical current density of the samples was estimated from the magnetic hysteresis loop using the extended critical state model [15].

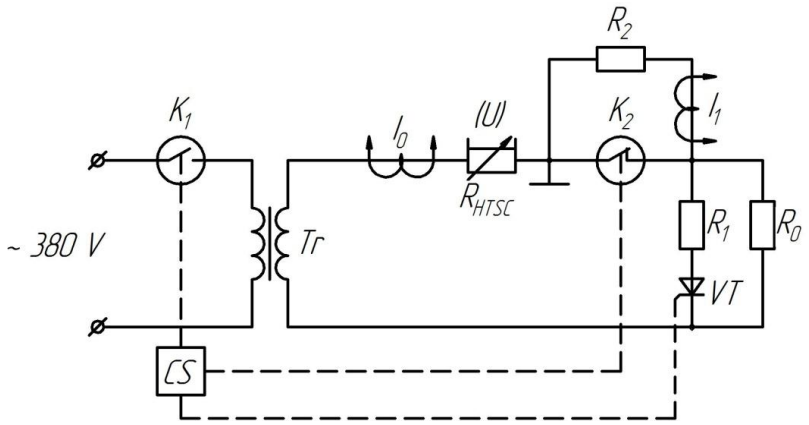

Fig. 1. Electrical circuit of the testing equipment

Figure 2 shows the X-ray patterns of $Y_1Ba_2Cu_3O_{7-\delta}$ + CuO composites with different concentrations of CuO nanopowder for 2θ values in the range from 30 to 90 degrees.

The XRD picture clearly illustrates that reflexes from CuO in the composites correspond to the reflexes characteristic of massive crystallites. Thus, the temperature conditions of composites annealing lead to a partial recrystallization of copper oxide. Debye X-ray patterns of the composites represent a superposition of reflections from the CuO and $YBa_2Cu_3O_{7-\delta}$ structures. No additional reflections were observed in the experiment, which indicated the absence of chemical interaction of CuO with the $YBa_2Cu_3O_{7-\delta}$ superconductor. In the 2θ range from 31.2 to 40 degrees, a monotonic increase in the reflection intensities was observed at 2θ = 35.559 degrees (-1-1 1) and at 2θ = 38.754 degrees (111) with an increase in the CuO content.

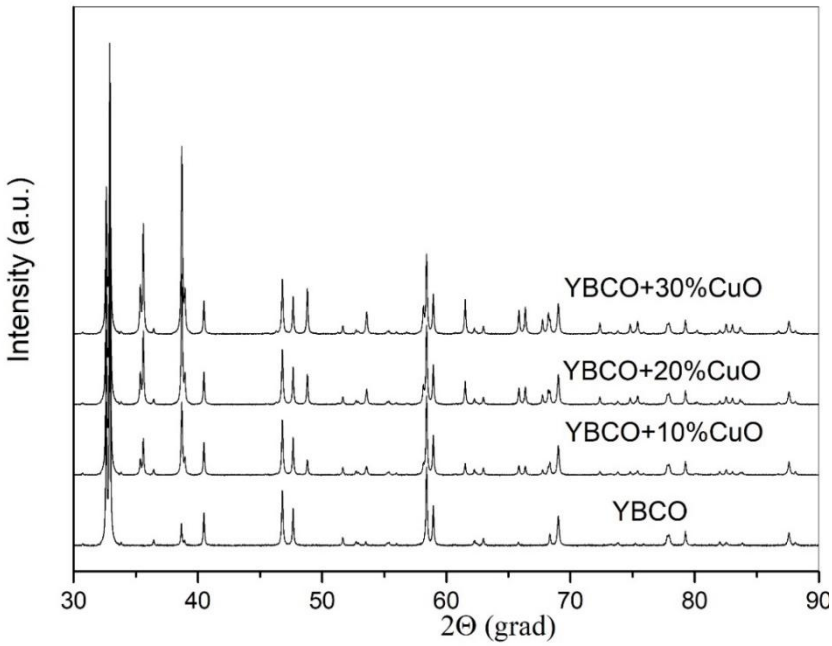

Figure 2 X-ray patterns of $Y_1Ba_2Cu_3O_{7-\delta}$ + CuO composites with different concentrations of CuO nanopowder

Figure 3 shows the dependence of the critical current density in samples on the magnetic field at T = 77 K calculated from the dependence of the nonequilibrium magnetization $\Delta M(H)$ on the hysteresis width along the axis M.

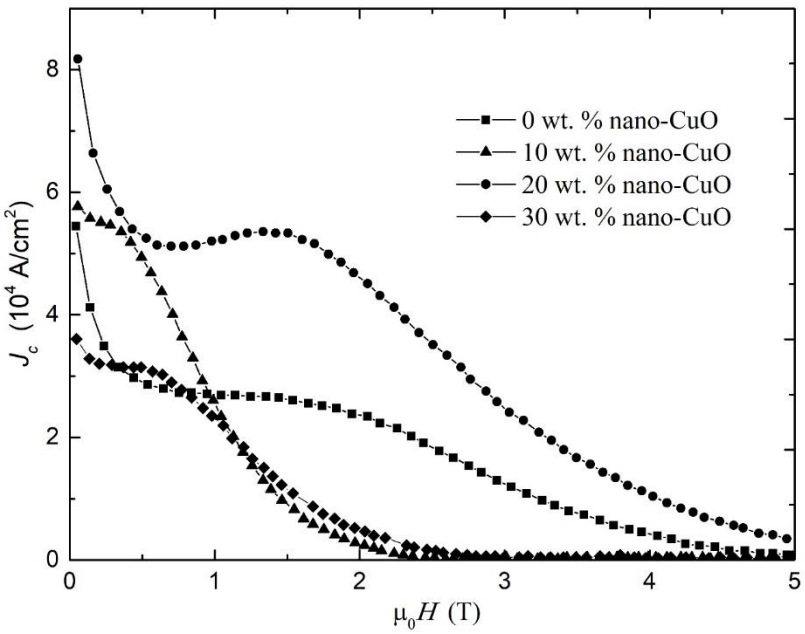

Fig.3. The dependence of the critical current density in samples on the magnetic field at T = 77 K

The hysteresis magnetization loop of superconducting granules is defined as $M_S(H) = M(H) - M_N(H)$. The critical current density J_c was determined in accordance with the equation:

$$J_c = 3\Delta M_S/2R,$$

where ΔM_S - nonequilibrium magnetization of superconducting granules, $\Delta M_S = \Delta M \times 100/(100\text{-}x)$, R - current circulation radius. The value of R depends on the magnetic field. In small fields (less than 100 Oe), R is equal to the radius of the sample [15]. In high fields, the superconductivity of grain boundaries is completely suppressed by the magnetic field, and the magnetic properties of a polycrystalline sample can only be determined by magnetization of the granules. Thus, when $H >$ 100 Oe, the value of R is equal to the average radius of the granules. Equation (1) enables us to calculate the intragranular density of the critical current for magnetization loops, measured to large fields. The averaged radius of granules $R \sim 2$ μm was determined from micrographs of the samples. The extended model of the critical state allows us to obtain more accurate estimates of R from the asymmetry of the magnetization loop relative to the H axis. The measured magnetization loops of different samples have different asymmetry. The asymmetry of the magnetization loop is determined by the ratio of penetration depth of the magnetic field λ to the radius of the granule. From the extended critical statistical model, we can conclude that $J_c = j_c (1\text{-}l / R) 3$, where j_c is the critical current density of the sample with R >> λ. The following equation is applied to the sample with $R >> \lambda$: $\Delta M_S = 2M_{up}S$, where $M_{up}S$ is the branch of the magnetization loop of superconducting granules in the increasing field. Thus, the equation should look as follows:

$$l/R = 1 - (\Delta M_S/2M_{up}S)1/3.$$

For $l = \lambda = 200$ nm for YBCO this equation was used to determine R. The values of ΔM_S and $M_{up}S$ were measured in the field $H_p \sim 5000$ Oe. The value of H is approximately equal to the value of the field of full penetration of the magnetic flux into the granules at a given temperature. For $H<H_p$, the expression of the critical state model for determining J_c gives understated values [15]. The estimation of the circulation radius shows that the average granule size increases from $R = 1.9$ μm (in the sample with $x = 0$) to $R = 2.7$ μm (in the sample with $x = 10\%$). With further increase in x, the values of R decrease to 2.1–2.2 μm in the samples with $x \geq 20\%$.

The samples of $YBa_2Cu_3O_{7-\delta}$/CuO composites with 10 wt.% of nano-CuO show some increase in current density J_c with a magnetic field B in the range from 0 to 1 T, which indicates an increase in magnetic flux pinning due to non-superconducting inclusions (Figure 3). They lead to distortions of the crystal structure at the interface and influence the distribution of oxygen-deficient areas, and also they increase the number of microregions with low J_c. However, a further increase in the magnetic field practically leads to an abrupt decrease in the current density down to 0. In this range of magnetic fields, dissipation follows the Arrhenius law $R \approx \exp(U(H)/T)$, characteristic of the model of magnetic flux creep with temperature-independent pinning energy $U(H)$ [16]. The samples of $YBa_2Cu_3O_{7-\delta}$/CuO composites with 20 wt.% of nano-CuO demonstrate a significant increase in the critical current density J_c in the entire range of the applied magnetic field B (Figure 3). In addition, in the range of magnetic fields B from 1 to 2 T, the samples show a clear peak effect. The models of increasing the transition temperature in superconductor volume (T_c), caused by defects in the crystal, which cause long-range deformations, are presented in [17]. It was shown that the effect of deformations, introduced by defects and changing T_c, increases noticeably in HTSC due to an increase in the coherence length and a strong anisotropic dependence of the volume Tc values on pressure [18]. Deformations, concerned with whisker defects, can be quite strong, causing local plastic deformations or structural transformations around dislocation arrays. The increase in T_c can be estimated for edge dislocations [19, 20], small-angle grain boundaries and metastable linear dislocation arrays, taking into account the anisotropic deformation dependence of

T_c in the ab plane and the proximity effect, which determines the superconducting state at intercrystallite boundaries. In addition, changes in $YBa_2Cu_3O_{7-\delta}$/CuO composites with 20 wt% of CuO, due to the strain fields of defects and the effect of changing T_c, influences the magnetic flux pinning and magnetic granularity.

The results of studying the produced composites and their application as a resistive current limiter are shown in Figures 4-5.

After the contactor K_1 was turned on, a load current began to flow in the circuit (the first one and a half periods), the amplitude of which (155 A) was about 2 times less than that of the critical current I_c. To demonstrate the effect of limiting the fault current, oscillographic testing of the current was carried out with simulation of fault current appearance without an HTSC element. In this case, a current i_{kz} with an aperiodic component of 4700 A amplitude flowed in the circuit. With HTSC present, the current in the circuit was limited due to a nonlinear increase in the resistance of the superconductor after its transition to the normal (non-superconducting) state. The limiting current I_{max} was determined by the degree of HTSC heating during the current half-wave.

Fig. 4 shows the current-limiting mode for the HTSC sample without addition of nano-dispersed CuO powder at $R_1 = 0$. Fig. 4 was obtained by superimposing oscillograms of the limiting current i_{lim} and voltage on the HTSC and oscillograms of the fault current I when no HTSC are present in the sample. In this case, the depth of the current limiting was $i_{scc} / i_{lim} >> 7$.

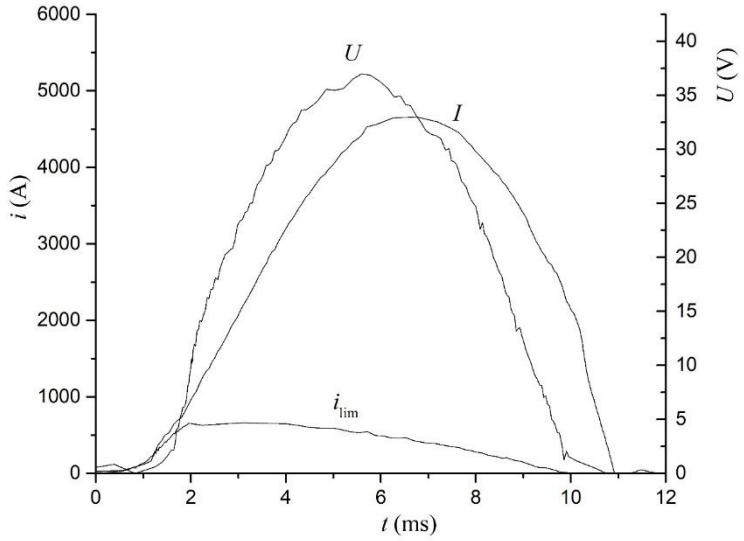

Fig. 4. Oscillograms of fault current I, limiting current i_{lim} and voltage U for a sample of HTSC without addition of nano-dispersed CuO powder

The oscillograms of current and voltage with different weight additives of nano-dispersed CuO powder, obtained at $R_1 = 0$, are shown in Fig. 5.

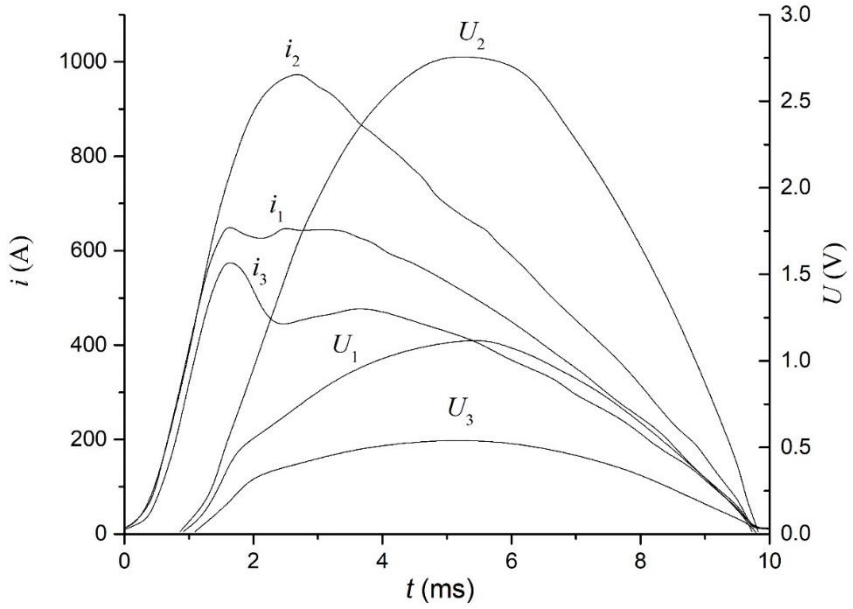

Fig. 5. Oscillograms of voltage and current for the sample of HTSC with different content of nano-dispersed powder CuO: *1* - 10 wt.%, *2* - 20 wt.%, *3* - 30 wt. %.

When the content of the nano-dispersed CuO powder increased, the character of changing the voltage and current on the sample coincided with the critical current calculated from the magnetization loops. Therewith, the delay in the moment of appearing the voltage on the HTSC element increased. A characteristic feature of the change in the current and the voltage over time is the presence of the moment at which a noticeable decrease in the rate of the current and the voltage rise occurred. This moment corresponds to the heating of the HTSC and the beginning of its transition to the normal state. The transition time of the HTSC from the superconducting to the normal state varied depending on the content of the nano-dispersed CuO powder from 1 ms to 1.5 ms.

Conclusion. Thus, it was found that the addition of nanosized CuO particles leads to an increase in the critical current density at T = 77 K for concentrations of 20 wt.%. Such an increase in the critical current can be explained by the presence of CuO nanoparticles that appear on the surface of superconducting granules. These granules become effective pinning centers for Abrikosov vortices. As the temperature rises, effective pinning occurs on larger CuO particles. The performed experiments demonstrated the ability to control the values of the critical current due to the addition of CuO nanoparticles as well as the effectiveness of the proposed approach to the problem of limiting and interruption of the short circuit current in AC circuits.

Acknowledgment. The work was performed with a support of the grant of the Russian Science Foundation (project no. 16-19-10054)

References

1. Leung E.M. Superconducting fault current limiters // IEEE Power Engineering Review. – 2000. – vol.20. – no.8. – pp. 15-18. doi: 10.1109/39.857449.

2. Paul W., Chen M., Lakner M., Rhyner J., Braun D., Lanz W. Fault current limiter based on high temperature superconductors – different concepts, test results, simulations, applications // Physica C: Superconductivity. – 2001. – vol.354. – no.1-4. – pp. 27-33. doi: 10.1016/s0921-4534(01)00018-1.

3. Joo M. Reduction of fault current peak in an inductive high-T_c superconducting fault current limiter // Cryogenics. – 2005. – vol.45. – no.5. – pp. 343-347. doi: 10.1016/j.cryogenics.2004.11.007.

4. Paul W., Chen M., Lakner M., Rhyner J., Widenhorn L., Guérig A. Test of 1.2 MVA high-T_c superconducting fault current limiter // Superconductor Science and Technology. – 1997. – vol.10. – no.12. – pp. 914-918. doi: 10.1007/978-4-431-66879-4_292.

5. Bock J., Breuer F., Walter H., Elschner S., Kleimaier M., Kreutz R., Noe M. CURL 10: development and field-test of a 10 kV/10 MVA resistive current limiter based on bulk MCP-BSCCO 2212 // IEEE Transactions on Applied Superconductiv-ity. – 2005. – vol.15. – no.2. – pp. 1955-1960. doi: 10.1109/tasc.2005.849344.

6. Elschner S., Breuer F., Noe M., Rettelbach T., Walter H., Bock J. Manufacturing and testing of MCP 2212 bifilar coils for a 10 MVA fault current limiter // IEEE Transactions on Applied Superconductivity. – 2003. – vol.13. – no.2. – pp. 1980-1983. doi: 10.1109/tasc.2003.812954.

7. Lepeshev, A.A. Magnetic properties and critical current of superconducting nanocomposites (1-x)$YBa_2Cu_3O_{7-\delta}$ + *x*CuO / A.A. Lepeshev, G.S. Patrin, G.Yu.Yurkin, A.D. Vasiliev, I.V. Nemtsev, D.M. Gokhfeld, A.D. Balaev, V.G. Demin, E.P. Bachurina, I.V. Karpov, A.V. Ushakov, L.Yu. Fedorov, L.A. Irtyugo, M.I. Petrov // Journal of Superconductivity and Novel Magnetism. – 2018. – Vol. 30, No 12, pp. 3351-3354. doi: 10.1007/s10948-018-4676-x.

8. Lepeshev, A.A. Particularities of the magnetic state of CuO nanoparticles produced by low-pressure plasma arc discharge / A.A. Lepeshev, A.V. Ushakov, I.V. Karpov, D.A. Balaev, A.A. Krasikov, A.A. Dubrovskiy, D.A. Velikanov, M.I. Petrov // Journal of Superconductivity and Novel Magnetism. – 2017. – Vol. 30, No 4, pp. 931-936. doi: 10.1007/s10948-016-3885-4.

9. Ushakov, A.V. Plasma-chemical synthesis of copper oxide nanoparticles in a low-pressure arc discharge / A.V. Ushakov, I.V. Karpov, A.A. Lepeshev, M.I. Petrov // Vacuum. – 2016. – Vol. 133, pp. 25-30. doi: 10.1016/j.vacuum.2016.08.007.

10. Ushakov, A. V. Peculiarities of magnetic behavior of CuO nanoparticles produced by plasma-arc synthesis in a wide temperature range / A.V. Ushakov, I.V. Karpov, A.A. Lepeshev // Journal of Superconductivity and Novel Magnetism. – 2017. – Vol. 30, No 12, pp. 3351-3354. doi: 10.1007/s10948-017-4311-2.

11. Ushakov, A.V. Specific Features of the Behavior of Electroarc CuO Nanoparticles in a Magnetic Field / A.V. Ushakov, I.V. Karpov, A.A. Lepeshev, M.I. Petrov, L.Yu. Fedorov // Physics of the Solid State. – 2015. – Vol. 57, No. 5, pp. 919–923. DOI: 10.1134/S1063783415050303

12. Ushakov, A.V. Copper Oxide of Plasma-Chemical Synthesis for Doping Superconducting Materials / A.V. Ushakov, I.V. Karpov, A.A. Lepeshev, L.Yu. Fedorov // International Journal of Nanoscience. – 2017. – Vol. 16, No. 4, p. 1750001. doi: http://dx.doi.org/10.1142/S0219581X17500016

13. Ushakov, A.V. Enhancing of magnetic flux pinning in $YBa_2Cu_3O_{7-x}$/CuO granular composites / A.V. Ushakov, I.V. Karpov, A.A. Lepeshev, M.I. Petrov // J. Appl. Phys. – 2015. – Vol. 118, No. 2, p.023907.

14. Karpov, I.V. Device for Increasing the Magnetic Flux Pinning in Granular Nanocomposites Based on the High-Temperature Superconducting Ceramic / I.V. Karpov, A.V. Ushakov, A.A. Lepeshev, L.Yu. Fedorov, E.A. Dorozhkina, O.N. Karpova, A.A. Shaikhadinov, V.G. Demin // Technical Physics. – 2018. – Vol. 63, No. 2, pp. 230-234. doi: 10.1134/S1063784218020196.

15. I.L. Landau, J.B. Willems, J. Hulliger, J. Phys.: Condens. Matter 20, 095222 (2008).

16. T.T.M. Palstra, B. Batlogg, R.B. van Dover, L.F. Schneemeyer, J.V. Waszczak Appl. Phys. Lett. 54, 763 (1989).

17. A. Gurevich, E.A. Pashitskii Phys. Rev. B. 56, 6213 (1997).

18. R.J. Wijngaarden, R. Griessen Studies on High Temperature Superconductors (edited by A.V. Narlikar, NovaScience: NewYork) 2, 29, (1989).

19. N. Browning, M.F. Chisholm, S.J. Pennycook, D.P. Norton, D.H. Lowndes Phys. C. 212, 185 (1993).

20. S.E. Babcock, J.L. Vargas Annual Rev. Mater. Sci. 25, 193 (1995).